Optical Materials 145 (2023) 114471

Contents lists available at ScienceDirect

Optical Materials

journal homepage: www.elsevier.com/locate/optmat

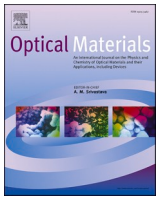

Research Article

# Understanding the suitable alloying conditions for highly efficient Cu- and Mn-doped $Zn_{1-x}Cd_xS/ZnS$ core-shell quantum dots

Manpreet Kaur [a,b,c], Ashma Sharma [b,d], Onur Erdem [b], Akshay Kumar [a,e], Hilmi Volkan Demir [b,d], Manoj Sharma [a,d,f,*]

[a] Department of Nanotechnology, Sri Guru Granth Sahib World University, Punjab, 140406, India
[b] Department of Electrical and Electronics Engineering, Department of Physics, and UNAM–Institute of Materials Science and Nanotechnology, Bilkent University, Ankara, 06800, Turkey
[c] Research and Development Cell, Central Instrumentation Facility (CIF), Lovely Professional University, Punjab, 144411, India
[d] LUMINOUS! Center of Excellence for Semiconductor Lighting and Displays, School of Electrical and Electronics Engineering, School of Physical and Mathematical Sciences, School of Materials Science and Engineering, Nanyang Technological University, Nanyang Avenue, 639798, Singapore
[e] Department of Physics, Sardar Patel University, Mandi, Himachal Pradesh, 175001, India
[f] ARC Centre of Excellence in Exciton Science, Department of Materials Science and Engineering, Monash University, Melbourne, Victoria, 3800, Australia

ARTICLE INFO

*Keywords:*
Colloidal quantum dots
Copper-doping
Manganese-doping
Alloying
Stoichiometric ratio

ABSTRACT

Doping of alloyed colloidal quantum dots (QDs) has garnered significant attention for providing tunable and Stokes-shifted emission. By alloying the host semiconductor nanocrystals (NCs), their band gap can be tuned. With the specific addition of dopant ions, these NCs can emit tunable emissions within the visible spectrum. However, while doped and alloyed quantum dots (QDs) have shown promise for tunable emissions, their emission qualities have not been consistent across the spectrum. Here, we report the synthesis of high-quality Cu- and Mn-doped $Zn_xCd_{1-x}S$ (x = 0–1) alloyed QDs by a colloidal non-injection method. In this study, we examined the effect of different dopant ions on the optical properties of similar alloyed nanocrystals. The deposition of a ZnS shell on these doped QDs significantly improves their quantum yield (QY), increasing it from 7.0 % to 50.0 % for Cu-doped QDs and from 30.0 % to 80.0 % for Mn-doped QDs. The Cu-doped QDs exhibit tunable emission from green to red across the visible spectrum by varying the Zn/Cd ratio, whereas the Mn-doped QDs show a fixed orange emission. Interestingly, the Cu-doped alloyed QDs show a contrasting trend in quantum yield (QY) compared to those of Mn-doped QDs when the amount of Cd in ZnCdS alloyed QDs is systematically changed. As the amount of Cd increases in the ZnCdS alloyed QDs, the Cu-doped QDs show both an increase in average lifetime and an increase in QY. In contrast, for the Mn-doped QDs, the decay lifetime values remain fairly constant for different amounts of Cd in the ZnCdS alloyed QDs, but the QY decreases as the amount of Cd increases. The results of this study may facilitate the design of optimal alloying combinations for Cu/Mn-doped QDs in optoelectronic applications.

## 1. Introduction

In recent years, there has been significant interest in doped colloidal quantum dots (QDs) due to their superior optical properties compared to undoped QDs. These include dopant-induced tunable emission in the visible to the near-infrared region, large Stokes shift [1], longer excited state lifetime [2] along with reduced self-absorption [3]. Whereas, undoped QDs achieve quantum confinement effect-induced tunable emission by the variation in size, shape, and dimensionality of the nanocrystals (NCs) [4]. Doped QDs possess potential applications in biomedical labeling or diagnostics [5,6], photovoltaic devices [7,8] and display or light-emitting devices [9,10]. However, the compatibility of the dopant ions with the host NCs is crucial for the successful positioning of the dopant ions into the crystal lattice. Among various transition metal ions doped QDs [11–15], Cu- and Mn-doped QDs have been considered efficient emitters in the visible region of the spectrum [16–18].

Furthermore, among semiconductor nanocrystals (NCs), doped

* Corresponding author. ARC Centre of Excellence in Exciton Science, Department of Materials Science and Engineering, Monash University, Melbourne, Victoria, 3800, Australia.
*E-mail address:* manoj.sharma@monash.edu (M. Sharma).

https://doi.org/10.1016/j.optmat.2023.114471
Received 28 May 2023; Received in revised form 21 August 2023; Accepted 6 October 2023
Available online 20 October 2023

binary (e.g. ZnS and CdS) QDs have gained particular importance due to their efficient ultraviolet-to-blue excitation [19–21]. In addition, to explore the emission tuning capability of these QDs by controlling their size, the advancement in their synthesis methods has led to the exploration of ternary QDs (e.g. ZnCdS, ZnInS, CuInS, etc.) which shows tunable optical properties by changing their stoichiometry [22–24]. Similar to binary QDs, the introduction of the dopant ions in these ternary QDs creates a mid-gap state within the bandgap which alters the resultant photoluminescence (PL) emission from excitonic to Stokes-shifted dopant-induced emission [25–27]. In this category, ZnCdS has been considered a suitable host as it exhibits a facilely tunable band gap by varying Zn/Cd stoichiometric ratio which is independent of size-dependent tuning [28]. Mn-doped ZnCdS QDs possess non-tunable emission which originates through $^4T_1$ - $^6A_1$ electronic transition (d-d transitions) states of $Mn^{2+}$ dopant ions which lie within the bandgap of host QDs [28], whereas Cu-doped ZnCdS QDs can provide tunable emission through the recombination of the electron present in the conduction band (CB) of host NC and hole present in Cu $T_2$ state [29,30]. For the case of Cu dopant emission, alloying in host semiconductor QDs varies the CB level which in turn tunes the emission spectrum. Therefore, the difference in the recombination process of Cu and Mn-doped QDs results in a different emission lifetime and spectral width [31,32]. In particular, Cu-doped $Zn_xCd_{1-x}S$ QDs show widely tunable emission from 400 to 700 nm by controlled variation of Zn/Cd ratio in the host systems. Besides, the PL QYs for these materials vary for the different colors [33]. However, Mn-doped $Zn_xCd_{1-x}S$ QDs show fixed orange emission for samples with variable Zn/Cd ratios [34] along with variable PL QY, full-width at half maximum (FWHM), and emission lifetimes [35]. To the best of our knowledge very less work has been done for the understanding of the variation in the alloying conditions for the same host semiconductor NC doped with Cu and Mn ions, respectively.

In this work, a simple non-injection method with slight amendments in previously reported recipes has been used to synthesize highly efficient Cu- and Mn-doped $Zn_xCd_{1-x}S$/ZnS core/shell QDs. The effect of different dopants on the optical properties of the same host NC has been studied in detail. The surface passivation of the QDs has been done with the shell of ZnS which suppresses the trap states and enhances the dopant emission, thus helping to improve the QY. The highest achieved QY for Cu-doped QDs after passivating with ZnS shell is ~50 % and for the Mn-doped ZnCdS/ZnS core/shell QDs synthesized by using the same method is ~80 %. The composition (i.e., Zn/Cd ratio) has been varied to achieve the tunable emission from the synthesized QDs. The Cu-doped QDs show tunable emission spectra from 490 nm to 600 nm in the visible region. On the other hand, the Mn-doped QDs show fixed emissions at 600 nm by changing the Zn/Cd ratio. It has been observed that the host NCs show comparatively different behavior for Cu and Mn dopants. The efficient emission of Cu-dopant is achieved by increasing the Cd content in the host ZnxCd1-xS/ZnS quantum dots, while efficient Mn emission is observed with lower Cd content in the same host material. This has been observed and understood by detailed optical studies using steady-state and time-resolved fluorescence (TRF) spectroscopy. The structural properties have been studied by using transmission electron microscopy (TEM), High-angle annular dark-field (HAADF) scanning transmission electron microscope (STEM), and X-ray diffraction (XRD) techniques.

## 2. Results and discussion

### 2.1. Cu-doped ZnCdS/ZnS QDs

The morphological analysis of the synthesized Cu-doped core and

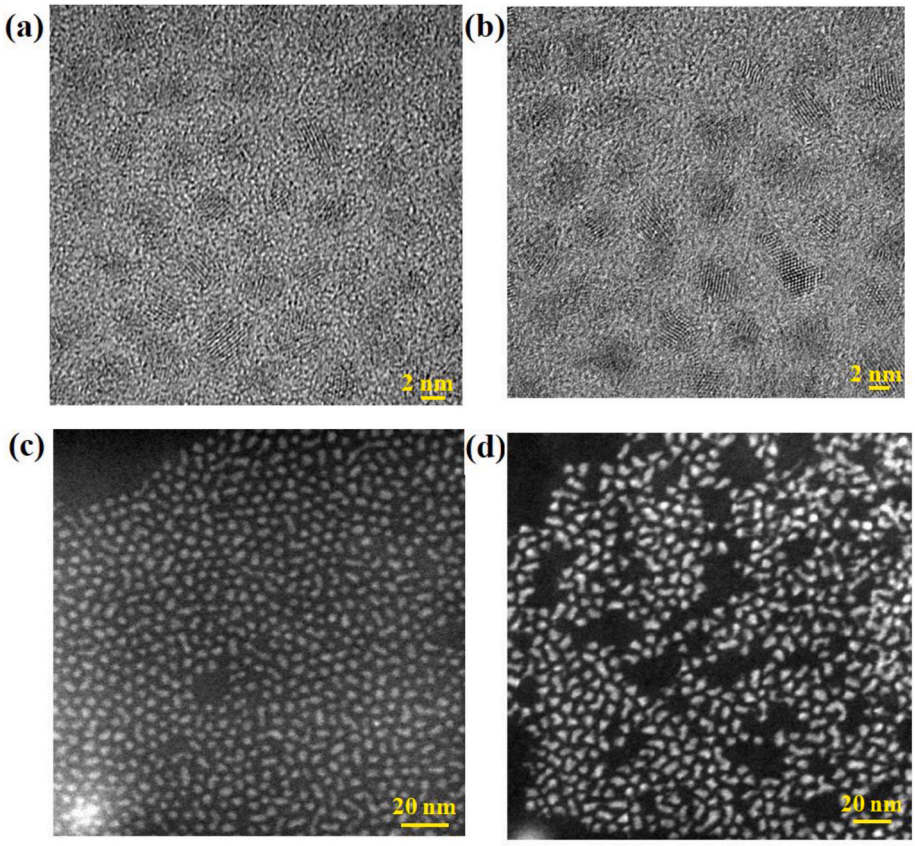


**Fig. 1.** (a) High-resolution transmission electron microscopy (HRTEM) images of ZnCdS: Cu (core) QDs, (b) ZnCdS: Cu/ZnS (core/shell) QDs and, morphology analysis of (c) ZnCdS: Cu (core) and (d) ZnCdS: Cu/ZnS (core/shell) by using STEM micrographs.

core/shell QDs with 1.0 % atomic weight of Cu-dopant has been done by using High-resolution transmission electron microscopy (HRTEM). The clear lattice fringes observed in the QDs indicate a high degree of crystallinity (Fig. 1a and b). The Scanning transmission electron microscopy (STEM) images of the Cu-doped ZnCdS/ZnS core and core/shell QDs have been shown in Fig. 1 (c) and (d) where atomic weight percentage of Cu-dopant is 1.0 % for all images. The average calculated size is approximately 3.5 nm and 6.0 nm for Cu-doped core and core/shell QDs, respectively. It has been observed that after depositing the ZnS shell over the core, the shape of the QDs diverts to non-uniform. The structural analysis of the synthesized QDs i.e., Cu-doped and Mn-doped ZnCdS/ZnS core/shell has been done by using X-ray diffraction (XRD). The broad XRD diffraction peaks have been depicted in Fig. S1. The synthesized QDs exhibit zinc blende (cubic) crystal structure as the peaks are located between the peaks of cubic ZnS and CdS materials (JCPDS index no. 241136) [36].

UV–visible absorbance and PL emission spectra of Cu-doped core- and core-shell QDs have been given in Fig. 2a. The absorbance spectra in the Cu-doped QDs show the characteristic excitonic transition of ZnCdS host NCs. The broad shoulder appearing in the absorbance spectrum is caused by the composition distribution in alloyed semiconductor QDs [37]. For Cu-doped QDs, the major emission peak arises near 635 nm, which is due to the recombination of electrons in the CB of the host material and the photoexcited holes in Cu $T_2$ states [38] The overall PL QY of the doped core is ~7 %. After that, a wide band gap material, i.e., ZnS, as a shell has been deposited over the doped core QDs. In literature, the ZnS shell has been observed to improve the optical properties and chemical stability of the core QDs [30]. In general higher bandgap inorganic shell material helps to passivate the surface trap states and increases the charge carrier confinement inside the core of QDs [39]. Similar to literature reports, deposition of ZnS shell on the doped core is observed to decrease the surface defects drastically following an increase of the PL QY to ~50 %. Further, Fig. 2a shows the 7 folds increase in overall PL QY of doped NCs with the deposition of the ZnS shell. Furthermore, with the deposition of the shell, the dopant-related PL peak shifts from 635 nm to 590 nm. A similar blue shift has been previously observed in literature for Cu-doped core-shell NCs [30]. This shift in emission wavelength has been accounted to the incorporation of the Zn ions into the crystal lattice which increases the Zn content in doped cores and hence increases the effective bandgap. Furthermore, a small blue shift in the bandgap is also apparent from the UV–visible absorption spectra after the deposition of the ZnS shell on the doped cores which further supports the blue shift in the dopant emission.

To understand the origin of emission in ZnCdS: Cu/ZnS core/shell QDs, the photoluminescence excitation (PLE) spectrum has been recorded and given in Fig. S2a. This has been collected in the wavelength range of 300 nm–600 nm for different emission wavelengths of broad dopant emission (i.e., at peak, red- and blue-tails). The corresponding emission wavelengths do not bring any major spectral difference in the PLE spectra. The PLE spectrum matches fairly well with the absorption spectrum (Fig. 2a). This shows that the efficient dopant emission results from the energy transfer from the host ZnCdS host QDs to Cu dopant states. The overlaid PLE, absorption, and PL emission spectra for core/shell QDs have been shown in Fig. S2b. Further, in order to understand the emission mechanism of Stokes-shifted emission in undoped and Cu-doped NCs, the steady-state absorption, emission, and lifetime characteristics of undoped ZnCdS/ZnS and Cu-doped ZnCdS/ZnS QDs are compared in Fig. S3, Table S1. The absorbance and PL spectra of the Cu-doped and undoped ZnCdS QDs are shown in Fig. S3 (a). Both ZnCdS: Cu/ZnS (doped) QDs and ZnCdS/ZnS QDs (undoped) exhibit broad emission peaks ~ 550 nm. The PL QYs of Cu-doped and undoped core-shell QDs are 50% and 5%, respectively. The doped QDs show Cu-mediated emission, whereas the emission from undoped QDs is attributed to the trap state-related emission. For more clarification, TRF measurements of both Cu-doped and undoped core/shell QDs have been performed (Fig. S3b). The PL decay components of doped and undoped QDs have been summarized in Table S1. The difference in emission pathways of doped and undoped QDs results in different PL decay lifetimes. The average PL lifetime for Cu-doped and undoped QDs are 815 ns and 348 ns, respectively. Furthermore, drop-casted solid films of doped and undoped QDs on a glass slide (Fig. S3c) were thermally annealed to 150 °C in ambient. It can be observed that at this temperature the doped QDs display a bright yellow emission whereas the undoped QDs do not show any emission. The shorter decay time, poor PL QYs, and lower thermal stability of undoped QDs' trap-related emission compared to doped QDs' dopant emission confirm their distinct origins.

Furthermore, the effect of dopant ions concentration on the optical properties of the host QDs has been studied by varying the dopant ion concentration during core synthesis. It has been found that the variation in the dopant ion concentration plays a significant role in changing the optical properties and the QY of the resulting doped QDs. The amount of Cu-dopant has varied from 0.05 % to 2.0 %. Fig. 2b shows that the change in concentration of Cu-dopant ions results in a small shift in the absorbance as well as PL emission spectra. This small shift may be due to the change in the particle size of the doped QDs by varying the Cu concentration. On the other hand, a change in doping percentage significantly affects the QY of doped core samples. The QY achieved for 0.05 %, 0.50 %, 1.00 %, and 2.00 % Cu-doped ZnCdS/ZnS core/shell QDs is 29 %, 20 %, 50 %, and 22 %, respectively. In this study, the highest QY achieved is 50 % for 1.0 % Cu-dopant concentration. However, further incorporation of Cu-ions may create additional non-radiative defect states which have resulted in a decrease in overall PL QY. This is similar to previous works on variation in Cu doping in alloyed ternary QDs [40]. The percentage incorporation of the Cu dopant has also been calculated from ICP-MS and given in Table S2.

The tunability in the PL emission peak of Cu-doped QDs has been

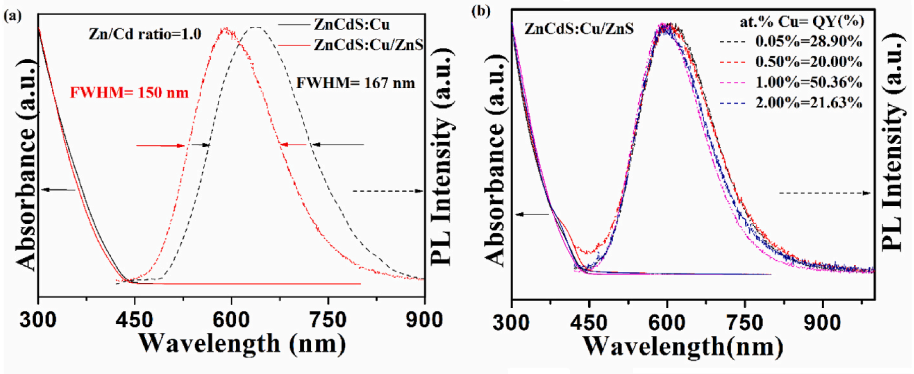


**Fig. 2.** (a) Normalized UV–visible absorption and PL spectra of ZnCdS:Cu (core) and ZnCdS:Cu/ZnS (core/shell) QDs, (b) UV–visible absorption and PL emission spectra of Cu-doped ZnCdS/ZnS core/shell QDs with varied Cu doping percentages.

achieved in alloyed semiconductor QDs by systematically altering the Zn/Cd ratio. The change in the composition of the alloyed host NCs alters the bandgap and the change in the CB edge of the host QDs tunes the PL peak position. Fig. 3 shows the UV–visible absorption spectra, PL emission spectra, and PL lifetime decay curves of Cu-doped ZnCdS QDs with different Zn/Cd stoichiometric ratios. With the increase in Zn concentration, the absorbance spectra show a blue shift (Fig. 3a) due to the increase in the incorporation of the higher band gap material ZnS (3.72 eV) [33]. However, with the increase in Cd concentration, the resultant band edge alters from the UV region to the visible region. The respective optical energy band gap for different samples has been calculated from their corresponding absorbance spectrum (inset Fig. 3a). This band gap engineering in the host QDs results in a shift in the PL peak position (Fig. 3b). It shows tunable emission which covers the green to the red region of the visible window (565–620 nm). Their respective FWHM also increases marginally with an increase in the concentration of Cd.

The PL decay lifetime for these synthesized QDs has been recorded by using FluoTime 200 time-correlated single photon-counting (TCSPC) instrument. The PL decay curves have been fitted by using a multi-exponential decay (Fig. 3c). The calculated average PL lifetime for samples synthesized using Zn/Cd stoichiometric ratios of 3.0, 1.0, and 0.33 are 224 ns, 815 ns, and 1063 ns at PL emission peaks of 505 nm, 548 nm, and 620 nm, respectively. Their respective lifetime parameters have been calculated and summarized in Table 1. Typically, the PL decay lifetime of the QDs depends on the size-dependent band gap, and intrinsic and surface defects involved in the PL emission [41,42]. Moreover, it is the combined effect of Cu-dopant emission along with trap state emission [42]. Here, the amplitude average decay lifetime of the Cu-doped QDs increases with a decrease in the Zn/Cd ratio at the constant dopant concentration. Briefly, as shown in Table 1, the percentage contribution of the largest lifetime component ($\tau_1$~1500–2500 ns) has been increased with the increase in Cd percentage in the host NCs. All other component's percentage contributions (except $A_1\tau_1$) are observed to decrease drastically with this increase in Cd values. Additionally, the fast component of 6.5 ns which can be attributed to the surface/deep trap states is nearly passivated in the samples possessing higher Cd content (e.g., Zn/Cd of 1.0 or 0.33). Furthermore, the PL QY is also observed to increase almost 2 times with an increase in the Cd concentration. Clearly, for these Cu-doped samples high content of Cd is favored for achieving high QY. The decrease in the QY generally results from the presence of the surface/deep trap states [30]. These synchronous variations in the average lifetimes and their components with changing Zn/Cd values suggest a possible correlation of the density of trap states with different Zn/Cd values in the presence of Cu-dopant ions. Therefore, a higher percentage of Cd in the host Cu-doped ZnCdS is observed to possess lesser trap states than those possessing higher Zn contents which is also supported by the observed average lifetime decay and quantum yield percentage (Fig. 3d).

### 2.2. Mn-doped ZnCdS/ZnS QDs

The morphological analysis of Mn-doped ZnCdS and ZnCdS/ZnS (core and core/shell) QDs has been performed by using STEM to study the effect of ZnS shell deposition on the shape and size of QDs. The average size calculated for Mn-doped core and core/shell QDs is approximately 4.2 ± 0.7 nm and 6.4 ± 0.8 nm respectively (Fig. 4 (a) and (b)). The high-quality monodispersed Mn-doped core QDs are nearly spherical in shape while the shape of core/shell QDs changes after depositing ZnS shell while monodispersity remains conserved.

The normalized absorbance and PL spectra of the as-synthesized Mn-doped QDs have been shown in Fig. 5a. The observed excitonic absorbance spectra are characteristic of ternary QDs. The incorporation of the Mn ions in the QDs generates its lower-lying energy states ($^4T_1$ - $^6A_1$) inside the energy band gap of the host semiconductor QDs. As a result, the photoexcited electron and hole pair generated by host NCs are transferred to $^4T_1$ and $^6A_1$ internal d-d transition states of Mn-dopant ions which result in Stokes-shifted and bright orange emission [43,44]. It is well known that the concentration of the dopant ions in the host NC plays a vital role in determining its optical properties [45]. Therefore, for Mn-doped QDs, the concentration of dopant ions has been varied from 0.25 % to 1.50 % (Fig. 5a). The achieved QYs for core ZnCdS: Mn QDs are 20 %, 24 %, 30 %, and 19 % for Mn concentrations of 0.25 %, 0.50 %, 1.0 %, and 1.50 %, respectively. The percentage

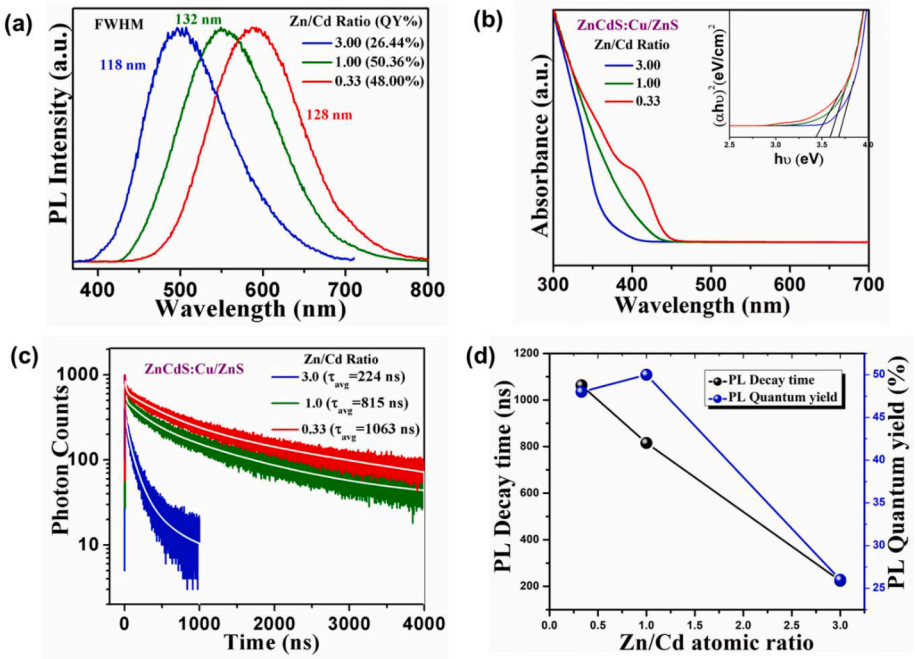


**Fig. 3.** (a) UV–visible absorption and (b) photoluminescence spectra of ZnCdS:Cu/ZnS core/shell QDs as a function of Zn/Cd stoichiometric composition. The inset in (a) shows the calculated energy band gap of ZnCdS:Cu/ZnS QDs, (c) PL decay curves of ZnCdS:Cu/ZnS QDs for different Zn/Cd ratios, and (d) Average PL lifetime and PL quantum yield with respect to change in Zn/Cd atomic ratio.

**Table 1**
Fluorescence decay components of the Cu-doped ZnCdS/ZnS QDs.

| Zn/Cd (nominal ratio) | TRF Decay Components | | | | | | | | Amplitude Average lifetime $\frac{\sum A_i\tau_i}{\sum A_i}$ |
|---|---|---|---|---|---|---|---|---|---|
| | $\tau_1$ (ns) | $\tau_2$ (ns) | $\tau_3$ (ns) | $\tau_4$ (ns) | $A_1$ | $A_2$ | $A_3$ | $A_4$ | $\tau_{avg}$ (ns) |
| 3.00 | 1546 | 412 | 6.5 | 98.2 | 43.3 | 217 | 374 | 132 | 224 |
| 1.00 | 2467 | 479 | 13.7 | 0 | 98.9 | 173 | 131 | 0 | 815 |
| 0.33 | 2752 | 515 | 17.1 | 0 | 251.0 | 360 | 216 | 0 | 1063 |

| Zn/Cd (Nominal ratio) | Fractional Emission Contributions $\frac{A_i\tau_i}{\sum A_i\tau_i}$ | | | | | | | |
|---|---|---|---|---|---|---|---|---|
| | $A_1\tau_1$ | $A_2\tau_2$ | $A_3\tau_3$ | $A_4\tau_4$ | $A_1\tau_1$ (%) | $A_2\tau_2$ (%) | $A_3\tau_3$ (%) | $A_4\tau_4$ (%) |
| 3.00 | 66941.8 | 89404 | 2431.0 | 12962.4 | 38.9 | 52.1 | 1.4 | 7.5 |
| 1.00 | 243986.3 | 82867 | 1794.7 | 0 | 74.2 | 25.2 | 0.5 | 0 |
| 0.33 | 690752.0 | 185400 | 3693.6 | 0 | 78.5 | 21.1 | 0.4 | 0 |

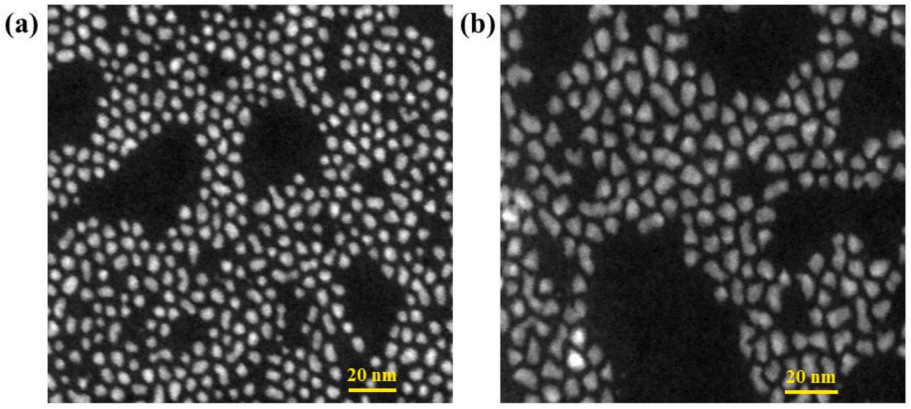


**Fig. 4.** STEM micrograph of (a) ZnCdS: Mn (core) and (b) ZnCdS: Mn/ZnS (core/shell) QDs. (Scale bar is 20 nm for both).

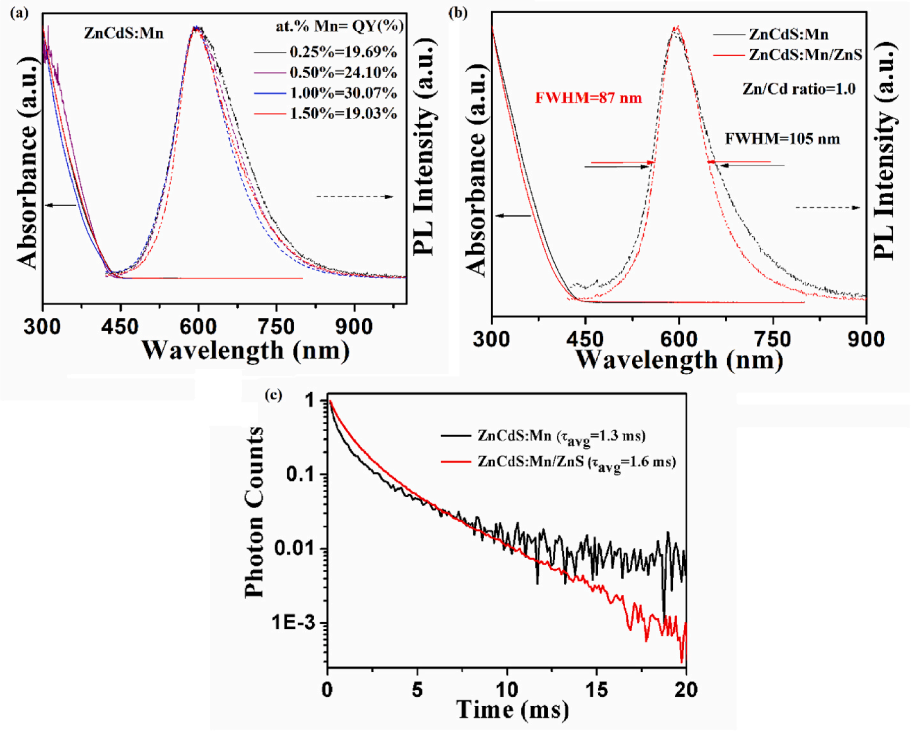


**Fig. 5.** (a) UV–visible absorption and PL spectra of ZnCdS: Mn (core) QDs with varied Mn doping percentages, (b) normalized UV–visible absorption and PL spectra of ZnCdS: Mn (core) and ZnCdS:Mn/ZnS (core/shell) QDs and (c) PL decay curves of ZnCdS: Mn/ZnS (core and core/shell) QDs at Zn/Cd stoichiometric ratio 1.0.

incorporation of the Mn dopant has also been calculated from ICP-MS and given in Table S3.

This highly intense orange PL emission peak appearing at 590 nm possesses an FWHM of 105 nm along with the highest PL QY of 30 % for our Mn (1.0 %) doped core-only QDs. Furthermore, the deposition of ZnS shell over these core Mn-doped ZnCdS QDs decreases the FWHM of dopant emission from 105 nm to 87 nm yielding a little narrower emission peak with a little spectral shift (Fig. 5b). In addition to the FWHM decrease, the QY increases drastically from 30 % to 75.0 %, which is comparable to the best achieved QY ever reported for this type of doped NCs [34]. The fluorescence decays of the core and core/shell QDs with 1.0 % atomic weight concentration of Mn-dopant have been recorded using a Cary Eclipse fluorescence spectrophotometer and fitted by using a bi-exponential decay (Fig. 5c). The calculated amplitude-averaged lifetime of the PL emission at 590 nm for ZnCdS: Mn (core) and ZnCdS: Mn/ZnS (core/shell) QDs is 1.3 and 1.6 ms, respectively (Table S4) where in both core and core/shell QDs, the atomic weight percentage of dopant is 1.0 %. The shell deposition increases the decay lifetime by eliminating the surface defect states. This is also supported by PL emission spectra in which there is a decrease in the value of FWHM after depositing the ZnS shell and an increase in the PL QY value. In order to investigate the origin of emission in these Mn-doped QDs, the photoluminescence excitation (PLE) spectrum for the emission at 590 nm has been recorded and shown in Fig. S4(a). The PLE spectrum has been obtained in the range of 300 nm–550 nm for different emission wavelengths (i.e., at peak, red- and blue-tails). The results reveal very little spectral difference in PLE spectra at different emission wavelengths. Thus, the QDs show reasonable monodispersity which has also been observed in TEM images. This indicates that the PL emission peak is simply due to Mn-dopant, which takes place via energy transfer from the ZnCdS host QDs to Mn-dopant transition states. Furthermore, the overlaid PLE, absorption, and PL emission spectra for core/shell QDs has been shown in Fig. S4(b). The excitation spectra obtained from the PLE measurements show similarity with the absorption spectra and provides Stokes-shifted dopant induced PL emission.

In order to study the different alloying conditions for Mn-doped QD hosts, the Zn/Cd ratio has been varied and their influence on the optical properties of ZnCdS: Mn/ZnS QDs has been studied. The Zn/Cd stoichiometric ratios of 0.33, 1.0, and 3.0 were investigated by keeping the Mn concentration constant. The absorption spectra reveal the effect of variation in concentration and it is red-shifted with increasing Cd concentration (Fig. 6a). The PL emission (Fig. 6b) for Mn-doped QDs arises due to the $^4T_1$-$^6A_1$ electronic transition of Mn-ions which is slightly affected by the change in Zn/Cd ratio [34]. However, there is an increase in FWHM (80 nm–96 nm) for Mn-doped QDs as the Zn/Cd ratio changes from 3.00 to 0.33. Interestingly, the increase in Zn content in NCs is observed to increase the PL QY of these Mn-doped NCs. Thus, a decrease in FWHM (96–80 nm) and an increase in PL QY (57–80 %) with an increase in Zn/Cd ratios suggest a decrease in non-radiative trap states with more zinc content in these alloyed NCs. This behavior is opposite to that of Cu-doped and alloyed ZnCdS NCs. The PL decay curves have been fitted by using a multi-exponential decay (Fig. S5a). The calculated average PL lifetime for a couple of Mn-doped QDs synthesized using Zn/Cd stoichiometric ratios of 1.0, and 0.33 are 1.60 ms, and 1.62 ms, respectively. However, unlike Cu-doped alloyed QDs, the average decay lifetime for Mn-doped QDs persists to be similar at different Zn/Cd ratios (Fig. S5a). As widely reported, this may be due to the different nature of Mn dopant emission as compared to Cu dopant emission within wide band gap semiconductor NCs [37,38,46]. For example, Mn dopant emission results from d-d transitions of Mn dopant ions where both electron and hole are transferred from host to Mn dopant d-d states. The average decay time and quantum yield values with respect to change in Zn/Cd ratio are shown in Fig. S5b which depicts the increase in QY with the increase of Zn content along with the average lifetime which remains almost the same even at higher Zn content for Mn-doped QDs. However, for Cu-dopant emission photo excited hole is transferred to the Cu (3d) state and the delocalized electron in the CB of host recombines the with the localized hole of Cu to generate Cu-dopant emission. The observed variable lifetime of Cu-doped QDs for different alloying conditions, in contrast to the non-variable lifetime of Mn-doped QDs, and opposite trends in QY for alloyed Cu/Mn-doped QDs suggests that changes in alloying conditions via significant variation in CB levels and suitability of different alloyed hosts for different ions. These results emphasize the critical role of suitable alloying conditions in achieving efficient dopant emission in the visible region of the spectrum.

## 3. Conclusion

In summary, we have synthesized high-quality Cu- and Mn-doped ZnxCd1-xS (x = 0–1) alloyed quantum dots using a colloidal non-injection method and studied the effect of different dopant ions on their optical properties. The deposition of a ZnS shell on these doped QDs significantly improves their quantum yield, with the highest achieved values of 50 % for the Cu-doped QDs and 80 % for the Mn-doped QDs. Our results show that the Cu-doped QDs exhibit tunable emission from green to red across the visible spectrum by varying the Zn/Cd ratio, while the Mn-doped QDs emit a fixed orange color. The tuning of the Zn/Cd ratio has been observed to play an important role in achieving the highest quantum yield. These findings provide insights into the suitable alloying conditions for the same host semiconductor NC doped with Cu and Mn ions, respectively. By understanding the effects of alloying on the optical properties of these materials, one can potentially design optimal alloying combinations for Cu/Mn-doped QDs in optoelectronic applications.

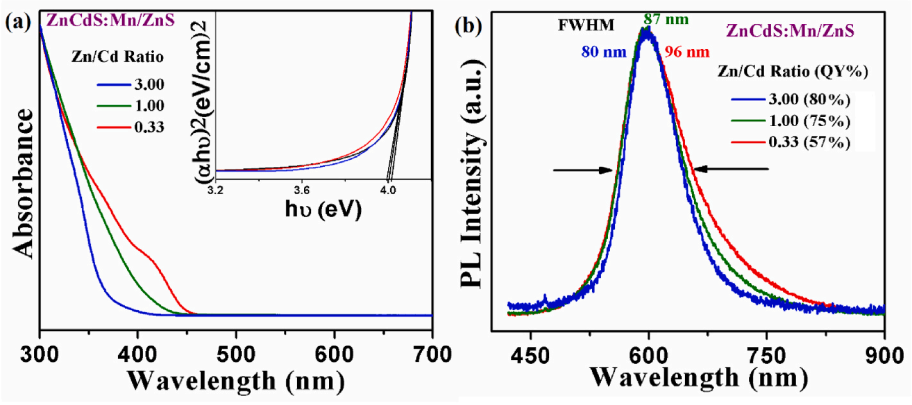


**Fig. 6.** (a) UV–visible absorption and (b) photoluminescence spectra of ZnCdS:Mn/ZnS core/shell QDs as a function of the Zn/Cd stoichiometric composition. The inset in (a) shows the calculated energy band gap of ZnCdS:Mn/ZnS QDs.

## 4. Experimental section

### 4.1. Chemicals used

Zinc acetate (Zn $(OAc)_2$, 99.99 %), cadmium oxide (CdO, 99.99 %), copper acetate (Cu$(OAc)_2$, 99.99 %), manganese acetate (Mn $(OAc)_2$, 98 %), sulfur powder (S, 99.99 %), dodecanethiol (DDT, 98 %), oleic acid (OA, 99 %), oleylamine (OAm, 70 %) and 1-octadecene (ODE, 90 %) were purchased from Sigma Aldrich. All the chemicals were used without any further purification. The synthesis of NCs was based on previously reported protocol through slight amendment [30].

### 4.2. Preparation of stock solutions

The stock solution of precursors was prepared before the start of the synthesis. The Zn stock solution or Zn oleate was prepared in a three-neck flask. The 0.1 M stock solution of Zn was obtained by dissolving 0.440 g (2 mmol) of Zn $(OAc)_2$ in 18.4 ml of ODE and 1.6 mL of OAm and degassed under vacuum at 95 °C for 30 min. Then under Argon (Ar) atmosphere, the temperature was raised to 160 °C and kept here for 5 min until a clear solution was obtained. For preparing 0.1 M Cd stock solution, 0.256 g (2 mmol) of CdO was dissolved in 16 mL ODE and 4 ml of OA. The solution was degassed under vacuum at 95 °C for 30 min. Then the temperature was raised to 160 °C under Ar atmosphere. The solution was retained here for 5 min to obtain a clear solution. The 0.01 M Cu stock solution was formulated by dissipation of 0.010 g (0.05 mmol) of Cu $(OAc)_2$ in 5.0 mL of OAm under stirring at 80 °C in the glove box. The 0.01 M Mn stock solution was prepared by dissolving 0.0086 g (0.05 mmol) of Mn $(OAc)_2$ in 5.0 mL of OAm under stirring at 80 °C inside the glove box. The 0.4 M sulfur stock solution (ODE-S) was obtained by dissolving 0.128 g of sulfur powder in 10 mL ODE by stirring at 140 °C.

### 4.3. Preparation of Cu-doped ZnCdS core QDs

The synthesis was carried out in Ar atmosphere. In the typical procedure, 2 mL of ODE and 1 mL of DDT were added to the three-neck flask. It was kept under a vacuum to remove oxygen and water. Then the reaction mixture was purged with Ar. Consequently, 1 mL of 0.1 M Zn-oleate (0.1 mmol), 1 mL of 0.1 M Cd-oleate (0.1 mmol), 0.2 mL of 0.01 M Cu stock solution (0.002 mmol), 1 mL of ODE-S (0.4 mmol) solution was added. Then the reaction mixture was heated to 220 °C. It takes 15 min to reach this temperature. The reaction mixture was kept at this temperature for 20 min under Ar flow. When the QDs growth was completed, the reaction mixture was cooled to 60 °C, and 10 mL of toluene was added afterward. The precipitation of as-synthesized NCs was done by adding excess ethanol into the toluene solution and centrifuging at 10000 rpm for 10 min. The purification was done by repeated precipitation and re-dispersion of NCs. The purified NCs were re-dispersed in toluene for further characterization.

### 4.4. Deposition of the ZnS shell over the core QDs

The ZnS shell was deposited over the crude Cu-doped ZnCdS QDs. The ZnS shell deposition was started over the crude reaction mixture after its growth time of 20 min. The shelling procedure was executed at the same temperature i.e., 220 °C. For the ZnS shell, the 3 mL of 0.4 M stock solution of the zinc precursor was injected into the reaction mixture. It was added in portions of 0.75 mL drop by drop at a time interval of 15 min. The purification method for ZnCdS:Cu/ZnS is similar to that of crude NCs.

### 4.5. Preparation of Mn-doped ZnCdS core QDs

The Mn-doped ZnCdS QDs were synthesized using the above procedure. In this, 0.1 mL of 0.01 M Mn stock solution was added in place of Cu stock solution into the reaction mixture and heated to 230 °C. The purification method was the same as used for Cu-doped ZnCdS QDs.

### 4.6. Deposition of the ZnS shell over the core QDs

The ZnS shell was deposited over the crude Mn-doped ZnCdS QDs. After the growth time of 20 min at 230 °C, the deposition of the shell started. The shelling procedure and purification method of ZnCdS: Mn/ZnS was similar to that of ZnCdS: Cu/ZnS QDs.

### 4.7. Material characterization

Absorbance and photoluminescence (PL) spectra were recorded by Varian-Cary 100 UV–visible spectrophotometer and Cary Eclipse fluorescence spectrophotometer. The quantum yield (QY) of the as-synthesized QDs was calculated by using the de Mello method [47]. The spectral results were acquired by using a monochromator-integrated xenon lamp with an excitation wavelength of 400 nm, a Hamamatsu integrating sphere, and an Ocean Optics Maya 2000 spectrometer. Transmission electron microscope (TEM) images were obtained from FEI Tecnai Osiris transmission electron microscopy which reveals the shape and size of QDs. X-ray diffraction (XRD) patterns of the QDs were collected by an XRD spectrometer with a Cu Kα line of 0.15418 nm. Lifetime measurements for Cu-doped QDs were taken with FluoTime 200 time-correlated single photon-counting (TCSPC) system. PL decay curves were analyzed using FluoFit software and fitted as multiexponential decays in deconvolution mode. Lifetime measurements and analyses for Mn-doped QDs were done by the Cary Eclipse fluorescence spectrophotometer. All the lifetime measurements were conducted in solution form using a quartz cuvette at room temperature.

## CRediT authorship contribution statement

**Manpreet Kaur:** synthesized the nanocrystals and conducted photophysical studies, All authors contributed to the, Data curation, data, Formal analysis, analysis, and scientific discussion, All authors read and approved the final manuscript. **Ashma Sharma:** helped in the synthesis and optical and structural measurements, All authors contributed to the, Data curation, data, Formal analysis, analysis, and scientific discussion, All authors read and approved the final manuscript. **Onur Erdem:** has conducted the lifetime measurements. **Akshay Kumar:** provided useful suggestions, All authors contributed to the, Data curation, data, Formal analysis, analysis, and scientific discussion, All authors read and approved the final manuscript. **Hilmi Volkan Demir:** conceived the project and, Supervision, the whole work, All authors contributed to the, Data curation, data, Formal analysis, analysis, and scientific discussion, All authors read and approved the final manuscript. **Manoj Sharma:** conceived the project and, Supervision, the whole work, All authors contributed to the, Data curation, data, Formal analysis, analysis, and scientific discussion, All authors read and approved the final manuscript.

## Declaration of competing interest

The authors declare that they have no known competing financial interests or personal relationships that could have appeared to influence the work reported in this paper.

## Data availability

Data will be made available on request.

## Acknowledgement

M.S. acknowledge funding through the Australian Research Council

Center of Excellence in Exciton Science (Grant No. CE170100026). H.V. D. acknowledges financial support in part from the Singapore Agency for Science, Technology and Research (A*STAR) MTC program under grant number M21J9b0085, Ministry of Education, Singapore, under its Academic Research Fund Tier 1 (MOE-RG62/20). H.V.D. also acknowledges support from TUBA and TUBITAK 2247-A National Leader Researchers Program (121C266). O.E. acknowledges the support of TUBITAK through BIDEB 2211 program. M.K. would like to acknowledge the University Grant Commission (UGC), India, for providing financial support (MANF-SRF).

## Appendix A. Supplementary data

Supplementary data to this article can be found online at https://doi.org/10.1016/j.optmat.2023.114471.

## References

[1] M. Liu, N. Yazdani, M. Yarema, M. Jansen, V. Wood, E.H. Sargent, Colloidal quantum dot electronics, Nat Electron 4 (2021) 548–558, https://doi.org/10.1038/s41928-021-00632-7.
[2] P. Wu, X.-P. Yan, Doped quantum dots for chemo/biosensing and bioimaging, Chem. Soc. Rev. 42 (2013) 5489–5521, https://doi.org/10.1039/C3CS60017C.
[3] N. Pradhan, X. Peng, Efficient and color-tunable Mn-doped ZnSe nanocrystal emitters: control of optical performance via greener synthetic chemistry, J. Am. Chem. Soc. 129 (2007) 3339–3347, https://doi.org/10.1021/ja068360v.
[4] D. Thomas, H.O. Lee, K.C. Santiago, M. Pelzer, A. Kuti, E. Jenrette, M. Bahoura, Rapid microwave synthesis of tunable cadmium selenide (CdSe) quantum dots for optoelectronic applications, J. Nanomater. 2020 (2020), 5056875, https://doi.org/10.1155/2020/5056875.
[5] T.S. Kanchana, T. Sivakumar, P. Venkateswari, Enhanced photocatalytic properties of ZnS/CdS/ZnCdS catalysts under visible light irradiation, J. Mol. Struct. 1265 (2022), 133375, https://doi.org/10.1016/j.molstruc.2022.133375.
[6] C.M. Tyrakowski, P.T. Snee, A primer on the synthesis, water-solubilization, and functionalization of quantum dots, their use as biological sensing agents, and present status, Phys. Chem. Chem. Phys. 16 (2014) 837–855, https://doi.org/10.1039/C3CP53502A.
[7] A.J. Nozik, M.C. Beard, J.M. Luther, M. Law, R.J. Ellingson, J.C. Johnson, Semiconductor quantum dots and quantum dot arrays and applications of multiple Exciton generation to third-generation photovoltaic solar cells, Chem. Rev. 110 (2010) 6873–6890, https://doi.org/10.1021/cr900289f.
[8] Z. Yang, C.-Y. Chen, P. Roy, H.-T. Chang, Quantum dot-sensitized solar cells incorporating nanomaterials, Chem. Commun. 47 (2011) 9561–9571, https://doi.org/10.1039/C1CC11317H.
[9] X. Yuan, J. Hua, R. Zeng, D. Zhu, W. Ji, P. Jing, X. Meng, J. Zhao, H. Li, Efficient white light emitting diodes based on Cu-doped ZnInS/ZnS core/shell quantum dots, Nanotechnology 25 (2014), 435202, https://doi.org/10.1088/0957-4484/25/43/435202.
[10] D.-Y. Jo, D. Kim, J.-H. Kim, H. Chae, H.J. Seo, Y.R. Do, H. Yang, Tunable white fluorescent copper gallium sulfide quantum dots enabled by Mn doping, ACS Appl. Mater. Interfaces 8 (2016) 12291–12297, https://doi.org/10.1021/acsami.6b01763.
[11] F. Chen, D. Gerion, L. Sciences, V. Di, L. Berkeley, Fluorescent CdSe/ZnS nanocrystal – peptide conjugates for long-term , nontoxic imaging and nuclear targeting in living cells, Nano Lett. 4 (2004) 1827–1832.
[12] N.S. Karan, S. Sarkar, D.D. Sarma, P. Kundu, N. Ravishankar, N. Pradhan, Thermally controlled cyclic insertion/ejection of dopant ions and reversible zinc blende/wurtzite phase changes in ZnS nanostructures, J. Am. Chem. Soc. 133 (2011) 1666–1669, https://doi.org/10.1021/ja109625v.
[13] R. Zeng, M. Rutherford, R. Xie, B. Zou, X. Peng, Synthesis of highly emissive Mn-doped ZnSe nanocrystals without pyrophoric reagents, Chem. Mater. 22 (2010) 2107–2113, https://doi.org/10.1021/cm9036023.
[14] B.T. Luong, E. Hyeong, S. Yoon, J. Choi, N. Kim, Facile synthesis of UV-white light emission ZnSe/ZnS:Mn core/(doped) shell nanocrystals in aqueous phase, RSC Adv. 3 (2013) 23395–23401, https://doi.org/10.1039/C3RA44154G.
[15] S. Mukherjee, J. Selvaraj, T. Paramasivam, Ag-doped ZnInS/ZnS core/shell quantum dots for display applications, ACS Appl. Nano Mater. 4 (2021) 10228–10243, https://doi.org/10.1021/acsanm.1c01720.
[16] J. Zhu, S. Mei, W. Yang, G. Zhang, Q. Chen, W. Zhang, R. Guo, Tunable emission of Cu (Mn)-doped ZnInS quantum dots via dopant interaction, J. Colloid Interface Sci. 506 (2017) 27–35, https://doi.org/10.1016/j.jcis.2017.06.043.
[17] R. P. K, R. Viswanatha, Mechanism of Mn emission: energy transfer vs charge transfer dynamics in Mn-doped quantum dots, Apl. Mater. 8 (2020), 020901, https://doi.org/10.1063/1.5140888.
[18] H. Nishimura, K. Enomoto, Y.-J. Pu, D. Kim, Hydrothermal synthesis of water-soluble Mn- and Cu-doped CdSe quantum dots with multi-shell structures and their photoluminescence properties, RSC Adv. 12 (2022) 6255–6264, https://doi.org/10.1039/D1RA08491G.
[19] Z. Bujňáková, E. Dutková, M. Kello, J. Mojžiš, M. Baláž, P. Baláž, O. Shpotyuk, Mechanochemistry of chitosan-coated zinc sulfide (ZnS) nanocrystals for bio-imaging applications, Nanoscale Res. Lett. 12 (2017) 328, https://doi.org/10.1186/s11671-017-2103-z.
[20] L. wei Liu, S. yi Hu, Y. Pan, J.Q. Zhang, Y.S. Feng, X.H. Zhang, Optimizing the synthesis of CdS/ZnS core/shell semiconductor nanocrystals for bioimaging applications, Beilstein J. Nanotechnol. 5 (2014) 919–926, https://doi.org/10.3762/bjnano.5.105.
[21] P.J. Thomas, G.L. Stansfield, N. Komba, D.J.H. Cant, K. Ramasamy, E. Albrasi, H. Al-Chaghouri, K.L. Syres, P. O'Brien, W.R. Flavell, others, Growth of nanocrystalline thin films of metal sulfides [CdS, ZnS, CuS and PbS] at the water–oil interface, RSC Adv. 5 (2015) 62291–62299.
[22] X. Wang, J. Damasco, W. Shao, Y. Ke, M.T. Swihart, Synthesis of Zn–in–S quantum dots with tunable composition and optical properties, ChemPhysChem 17 (2016) 687–691, https://doi.org/10.1002/cphc.201500746.
[23] Z. Bai, W. Ji, D. Han, L. Chen, B. Chen, H. Shen, B. Zou, H. Zhong, Hydroxyl-terminated CuInS2 based quantum dots: toward efficient and bright light emitting diodes, Chem. Mater. 28 (2016) 1085–1091, https://doi.org/10.1021/acs.chemmater.5b04480.
[24] M. Yang, Y. Wang, Y. Ren, E. Liu, J. Fan, X. Hu, Zn/Cd ratio-dependent synthetic conditions in ternary ZnCdS quantum dots, J. Alloys Compd. 752 (2018) 260–266, https://doi.org/10.1016/j.jallcom.2018.04.084.
[25] S. Bhandari, R. Begum, A. Chattopadhyay, Surface ion engineering for tuning dual emission of ZnxCd1−xS nanocrystals, RSC Adv. 3 (2013) 2885, https://doi.org/10.1039/c2ra22447j.
[26] D. Pan, D. Weng, X. Wang, Q. Xiao, W. Chen, C. Xu, Z. Yang, Y. Lu, Alloyed semiconductor nanocrystals with broad tunable band gaps, Chem. Commun. (2009) 4221–4223, https://doi.org/10.1039/b905151a, 0.
[27] X. Zhong, Y. Feng, W. Knoll, M. Han, Alloyed ZnxCd1-xS nanocrystals with highly narrow luminescence spectral width, J. Am. Chem. Soc. 125 (2003) 13559–13563.
[28] S. Cao, C. Li, L. Wang, M. Shang, G. Wei, J. Zheng, W. Yang, Long-lived and well-resolved Mn2+ ion emissions in CuInS-ZnS quantum dots, Sci. Rep. 4 (2014) 7510, https://doi.org/10.1038/srep07510.
[29] R. Zeng, R. Shen, Y. Zhao, X. Li, Aqueous synthesis of Cu-doped ZnCdS/ZnS core/shell nanocrystals with a new and highly reactive sulfur source, Nanotechnology 25 (2014) 135602–135610, https://doi.org/10.1088/0957-4484/25/13/135602.
[30] W. Zhang, X. Zhou, X. Zhong, One-pot noninjection synthesis of Cu-doped ZnxCd1-xS nanocrystals, Inorg. Chem. 51 (2012) 3579–3587.
[31] M. Kaur, A. Sharma, M. Olutas, O. Erdem, A. Kumar, M. Sharma, H.V. Demir, Cd-free Cu-Doped ZnInS/ZnS Core/Shell Nanocrystals : Controlled Synthesis and Photophysical Properties, 2018.
[32] M. Sharma, M. Olutas, A. Yeltik, Y. Kelestemur, A. Sharma, S. Delikanli, B. Guzelturk, K. Gungor, J.R. McBride, H.V. Demir, Understanding the journey of dopant copper ions in atomically flat colloidal nanocrystals of CdSe nanoplatelets using partial cation exchange reactions, Chem. Mater. 30 (2018) 3265–3275, https://doi.org/10.1021/acs.chemmater.8b00196.
[33] A. Yakoubi, T. Ben Chaabane, A. Aboulaich, R. Mahiou, L. Balan, G. Medjahdi, R. Schneider, Aqueous synthesis of Cu-doped CdZnS quantum dots with controlled and efficient photoluminescence, J. Lumin. 175 (2016) 193–202, https://doi.org/10.1016/j.jlumin.2016.02.035.
[34] I. Levchuk, C. Würth, F. Krause, A. Osvet, M. Batentschuk, U. Resch-Genger, C. Kolbeck, P. Herre, H.P. Steinrück, W. Peukert, C.J. Brabec, Industrially scalable and cost-effective Mn2+ doped ZnxCd1−xS/ZnS nanocrystals with 70% photoluminescence quantum yield, as efficient down-shifting materials in photovoltaics, Energy Environ. Sci. 9 (2016) 1083–1094, https://doi.org/10.1039/C5EE03165F.
[35] V. Nadtochenko, D. Cherepanov, S. Kochev, M. Motyakin, A. Kostrov, A. Golub, O. Antonova, Y. Kabachii, S. Rtimi, Structural and optical properties of Mn2+-doped ZnCdS/ZnS core/shell quantum dots: new insights in Mn2+ localization for higher luminescence sensing, J. Photochem. Photobiol. Chem. 429 (2022), 113946, https://doi.org/10.1016/j.jphotochem.2022.113946.
[36] S. Kumar, A.K. Chawla, N. Kumar, R. Chandra, High temperature powder diffraction study of (Zn,Cd)S and ZnxCd1−xS nanopowders, RSC Adv. 1 (2011) 1078–1082, https://doi.org/10.1039/C1RA00064K.
[37] Y.C. Li, M.F. Ye, C.H. Yang, X.H. Li, Y.F. Li, Composition- and shape-controlled synthesis and optical properties of ZnxCd1–xS alloyed nanocrystals, Adv. Funct. Mater. 15 (2005) 433–441, https://doi.org/10.1002/adfm.200400320.
[38] M. Sharma, K. Gungor, A. Yeltik, M. Olutas, B. Guzelturk, Y. Kelestemur, T. Erdem, S. Delikanli, J.R. Mcbride, Near-unity emitting copper-doped colloidal semiconductor quantum wells for luminescent solar concentrators, Adv. Mater. 29 (2017), 1700821, https://doi.org/10.1002/adma.201700821.
[39] Z. Fang, P. Wu, X. Zhong, Y.-J. Yang, Synthesis of highly luminescent Mn:ZnSe/ZnS nanocrystals in aqueous media, Nanotechnology 21 (2010), 305604.
[40] N.X. Ca, H.T. Van, P.V. Do, L.D. Thanh, P.M. Tan, N.X. Truong, V.T.K. Oanh, N. T. Binh, N.T. Hien, Influence of precursor ratio and dopant concentration on the structure and optical properties of Cu-doped ZnCdSe-alloyed quantum dots, RSC Adv. 10 (2020) 25618–25628, https://doi.org/10.1039/d0ra04257a.
[41] D. Choi, J.Y. Pyo, D.J. Jang, Impurity location-dependent relaxation dynamics of Cu:CdS quantum dots, Nanoscale Res. Lett. 12 (2017) 49, https://doi.org/10.1186/s11671-017-1832-3.
[42] N. Srivastava, B. B, S. Jana, Pradhan, Doping Cu in semiconductor nanocrystals: some old and some new physical insights, J. Am. Chem. Soc. 133 (2011) 1007–1015.
[43] A. Singh, R. Kaur, O.P. Pandey, X. Wei, M. Sharma, Synthesis of fluorescent core-shell nanomaterials and strategies to generate white light, J. Appl. Phys. 118 (2015), https://doi.org/10.1063/1.4927482.
[44] C.C. Lin, K.Y. Xu, D. Wang, A. Meijerink, Luminescent manganese-doped CsPbCl3 perovskite quantum dots, Sci. Rep. 7 (2017), 45906.

[45] S. Mabrouk, H. Rinnert, L. Balan, S. Blanchard, J. Jasniewski, G. Medjahdi, R. Ben Chaabane, R. Schneider, Aqueous synthesis of highly luminescent ternary alloyed Mn-doped ZnSeS quantum dots capped with 2-mercaptopropionic acid, J. Alloys Compd. 858 (2021), 158315, https://doi.org/10.1016/j.jallcom.2020.158315.

[46] B.B. Srivastava, S. Jana, N. Pradhan, Doping Cu in semiconductor nanocrystals: some old and some new physical insights, J. Am. Chem. Soc. 133 (2011) 1007–1015, https://doi.org/10.1021/ja1089809.

[47] J.C. de Mello, H.F. Wittmann, R.H. Friend, An improved experimental determination of external photoluminescence quantum efficiency, Adv. Mater. 9 (1997) 230–232, https://doi.org/10.1002/adma.19970090308.